Strain-Dependent Edge Structures in MoS_2 Layers

Tinoco Rivas, M.; Maduro, Luigi; Masaki, Mukai; Okunishi, Eiji; Conesa-Boj, Sonia

DOI
10.1021/acs.nanolett.7b03627

Publication date
2017

Document Version
Final published version

Published in
Nano Letters: a journal dedicated to nanoscience and nanotechnology

NANO LETTERS

Letter

pubs.acs.org/NanoLett

Strain-Dependent Edge Structures in MoS_2 Layers

Miguel Tinoco,[†] Luigi Maduro,[†] Mukai Masaki,[‡] Eiji Okunishi,[‡] and Sonia Conesa-Boj*[,†]

[†]Kavli Institute of Nanoscience, Delft University of Technology, 2628CJ Delft, The Netherlands

[‡]JEOL Ltd., 3-1-2 Musashino, Akishima, Tokyo 196-8558, Japan

Supporting Information

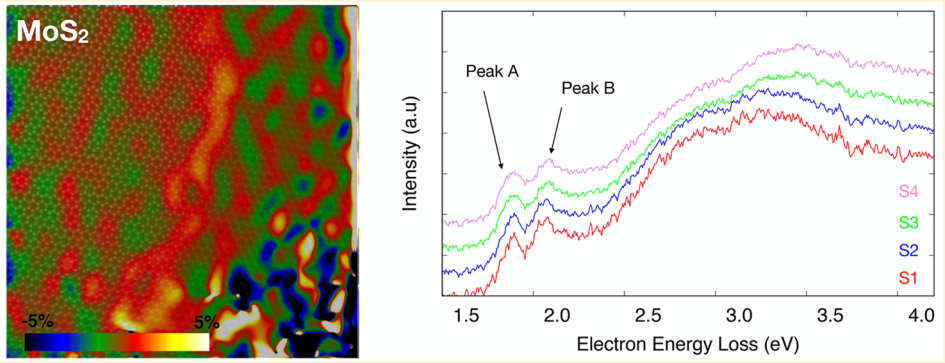

ABSTRACT: Edge structures are low-dimensional defects unavoidable in layered materials of the transition metal dichalcogenides (TMD) family. Among the various types of such structures, the armchair (AC) and zigzag (ZZ) edge types are the most common. It has been predicted that the presence of intrinsic strain localized along these edges structures can have direct implications for the customization of their electronic properties. However, pinning down the relation between local structure and electronic properties at these edges is challenging. Here, we quantify the local strain field that arises at the edges of MoS_2 flakes by combining aberration-corrected transmission electron microscopy (TEM) with the geometrical-phase analysis (GPA) method. We also provide further insight on the possible effects of such edge strain on the resulting electronic behavior by means of electron energy loss spectroscopy (EELS) measurements. Our results reveal that the two-dominant edge structures, ZZ and AC, induce the formation of different amounts of localized strain fields. We also show that by varying the free edge curvature from concave to convex, compressive strain turns into tensile strain. These results pave the way toward the customization of edge structures in MoS_2, which can be used to engineer the properties of layered materials and thus contribute to the optimization of the next generation of atomic-scale electronic devices built upon them.

KEYWORDS: *Transition-metal dichalcogenides, edge structures, strain, aberration-corrected transmission electron microscopy, electron energy loss spectroscopy*

Layered materials of the transition-metal dichalcogenides (TMDs) family have experienced an impressive boost in the recent years motivated by their striking physical functionalities. In particular, MoS_2 has become a very promising material exhibiting a wide range of possibilities in terms of applications from catalysis[1,2] to electronic[3−5] and optical[6,7] devices. For instance, when MoS_2 is thinned down to a single monolayer (ML), its indirect band gap switches to a direct band gap[8,9] of around 1.88 eV.

Recently, significant attention has been devoted to a specific type of low-dimensional defects, unavoidable in TMDs, known as the edge structures, which are also present in other important layered materials such as graphene.[10−13] These defects arise due to the lack of inversion symmetry in TMDs, which leads in turn to the formation of different edge configurations. Among the various types of possible edge terminations, the specific structures that exhibit a higher degree of symmetry are the so-called armchair (AC) and zigzag (ZZ) structures.

Remarkably, rather than representing a bottleneck for the customization of TMD-based devices, these edge structures allow the tailoring of their associated electronic properties[14,15] as well as their chemical reactivity.[16] For instance, carrier transport in graphene has been demonstrated to depend drastically on its specific edge structures.[17−19] Another example is provided by triangular MoS_2 nanocrystals deposited on Au (111) substrate,[20] which exhibit the presence of metallic edge modes in the ZZ terminations. These various features illustrate the potentialities of engineering edge structures in layered materials for application in electronics and optoelectronics.[21,22]

An important property that characterizes these edge structures is their intrinsic strain. In the case of graphene, it has been predicted that edges structures can be found under either compression or tension, depending on the specific type

Received: August 23, 2017
Revised: October 18, 2017
Published: October 24, 2017

DOI: 10.1021/acs.nanolett.7b03627
Nano Lett. 2017, 17, 7021−7026

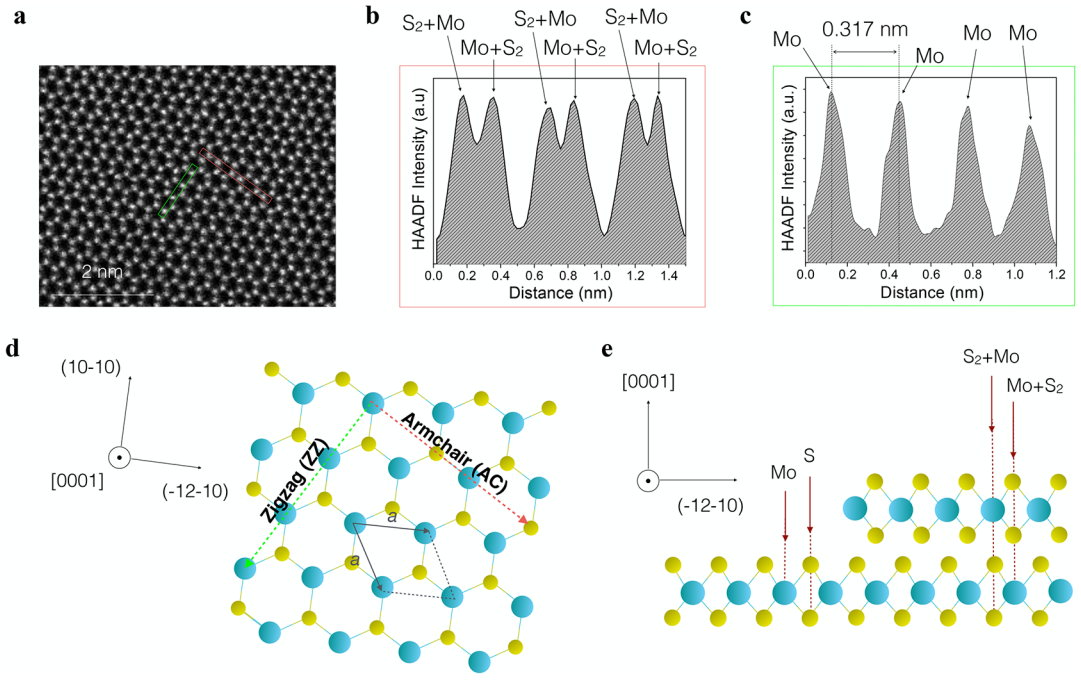

Figure 1. (a) Atomic-resolution STEM image of [0001]-oriented MoS_2 flake. (b, c) HAADF intensity profile taken along the AC and ZZ directions red and green rectangles in panel a, respectively. (d, e) Schematic atomic model of in-plane and out-of-plane of 2H MoS_2, respectively. In panel d, the AC and ZZ directions have been indicated by red and green dashed arrows, respectively.

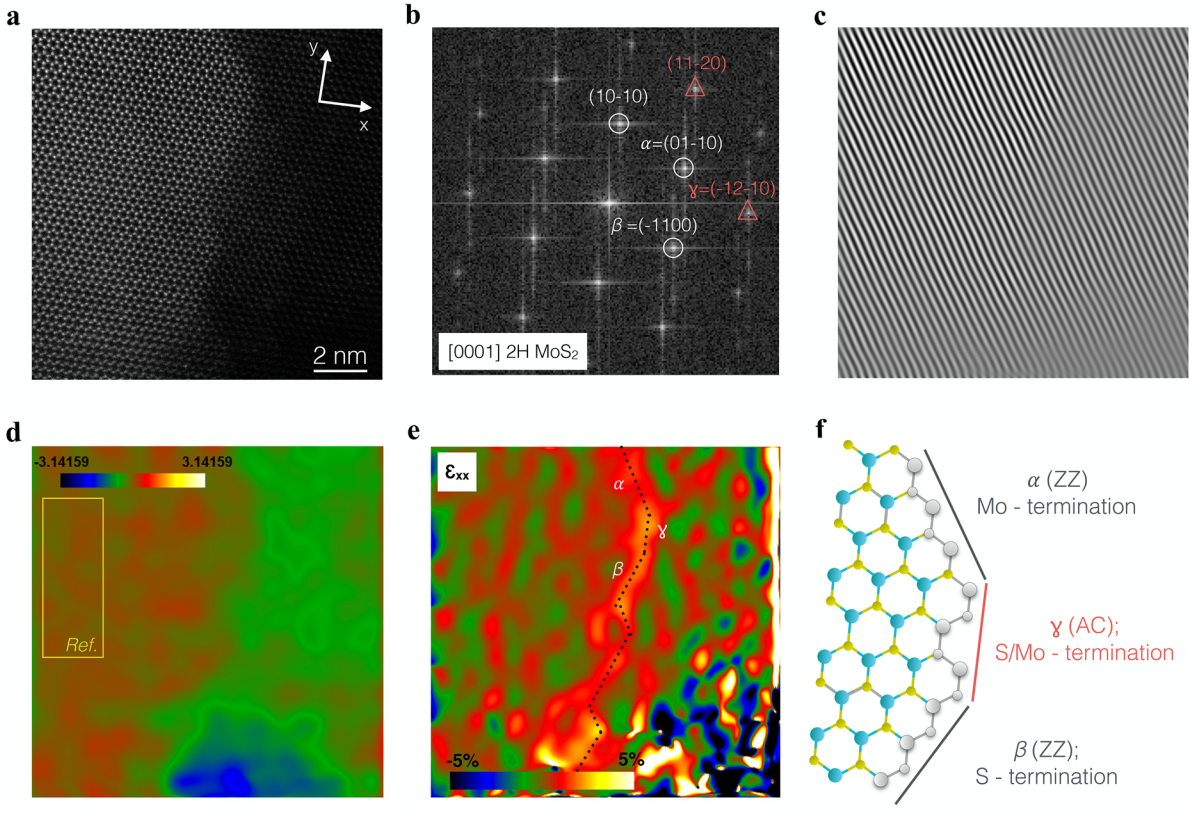

Figure 2. (a, b) Atomic-resolution HAADF image taken in the transition region between 3MLs and 2MLs and the corresponding fast Fourier transform (FFT), respectively. (c) (01−10) lattice fringes obtained by filtering. (d) Phase image of (01−10) lattice fringes, where the yellow rectangle indicates the reference region used for the strain field map calculation. The color range indicates variations from $-\pi$ to π. (e) The ε_{xx} strain component indicating the presence of strong tensile strain in this transition region. (f) Atomic model representing the structure of the ZZ and AC edge structures in MoS_2.

of edge structures.[12,13] However, most of these studies are limited to density functional theory (DFT) calculations. Therefore, there is an urgency to carry out an experimental program to validate these theoretical expectations. Moreover,

DOI: 10.1021/acs.nanolett.7b03627
Nano Lett. 2017, 17, 7021−7026

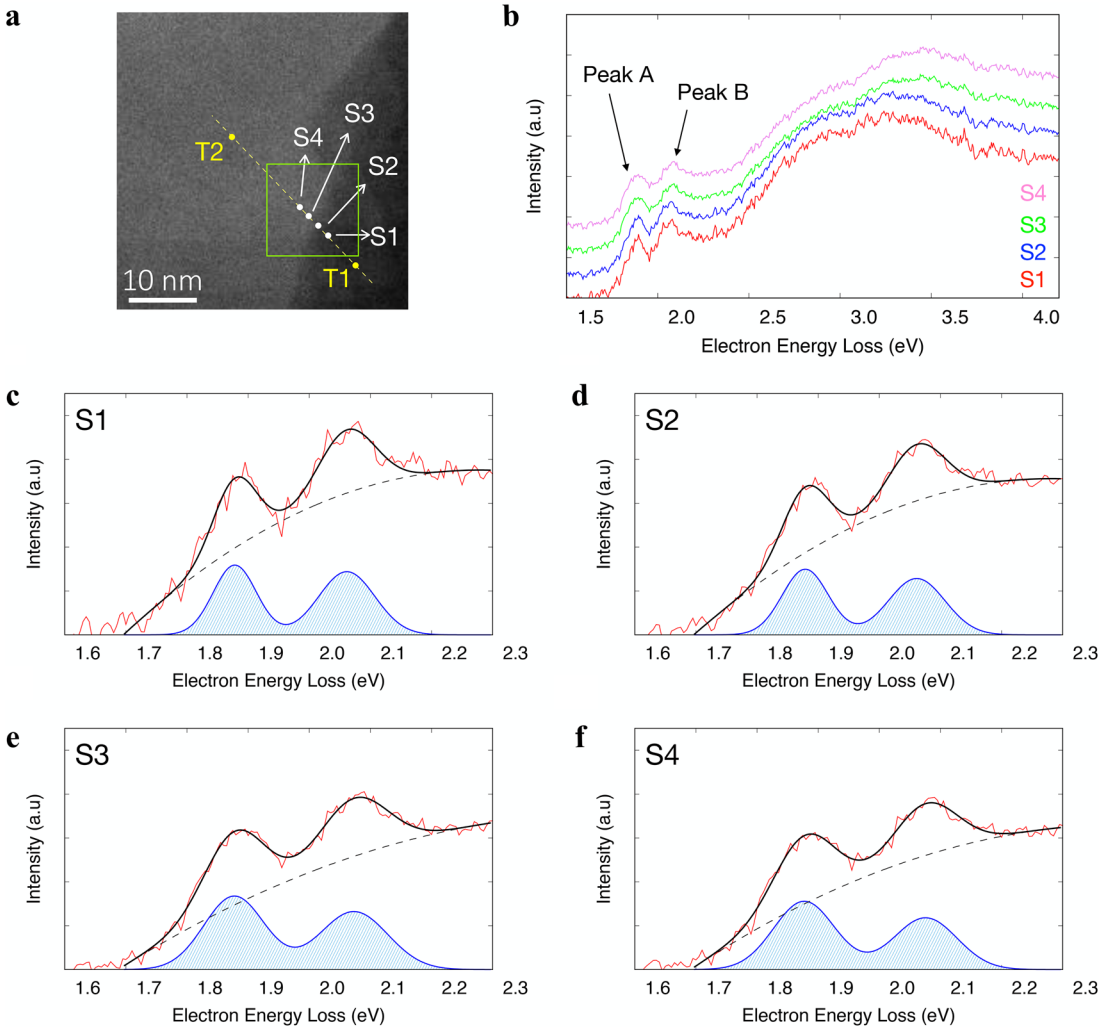

Figure 3. (a) Low-magnification HAADF−STEM image of the MoS_2 flake in the transition region between 2 and 3 ML. (b) Offset of the EELS spectra corresponding to S1, S2, S3, and S4 in panel a. (c−f) EELS spectra recorded at S1, S2, S3, and S4 with the corresponding fits.

although strain is a well-understood mechanism from the theoretical point of view, the experimental quantification of its effects in edge structures in MoS_2 has never been performed so far,[23] and thus its impact remains largely unexplored. Bridging this gap is therefore one of the main motivations of this work.

Here, we combine aberration-corrected transmission electron microscopy (TEM) with the geometrical-phase analysis (GPA) method to quantify the local strain field relaxation map in MoS_2 layers. Our results reveal that the two-dominant edge structures, AC and ZZ, induce the formation of different amounts of localized strain fields. The resulting improved knowledge about the edge morphology and properties in MoS_2 can in turn provide novel avenues (for instance, to tailor the carrier type and catalytic activity of layered materials), providing important input for the next generation of optoelectronic devices built upon them.

First of all, the crystalline nature of the MoS_2 flakes is determined by means of aberration-corrected high-angle annular dark-field scanning transmission electron microscopy (AC HAADF-STEM) characterization. For these studies, MoS_2 flakes are mechanically exfoliated and subsequently transferred to a TEM grid. For further details, see section I of the Supporting Information. Figure 1a displays a AC-STEM image of a representative MoS_2 flake, obtained by operating the microscope at 200 kV. The characteristic hexagonal honeycomb atomic arrangement of [0001]-oriented MoS_2 flake is clearly resolved. Together with the corresponding HAADF intensity profile (Figure 1b), which is directly related to the averaged atomic number and the thickness of the sample;[24] this confirms the hexagonal 2H crystalline phase of MoS_2. Note that here the HAADF intensity profile has been taken along the armchair (AC) direction (red rectangle in Figure 1a). For [0001]-oriented MoS_2 (Figure 1d), at the S-site, the electron beam interacts with a S atom first, while at the Mo site, the Mo atom is contacted first (Figure 1e). The fact that there are no variations in the relative intensities between the Mo-sites and S-sites indicates that in this specific region we have an even number of MoS_2 layers. The lattice parameter of MoS_2 can be then determined by measuring the Mo−Mo bond length, which can be measured from the HAADF intensity profile (Figure 1c) taken along the zigzag (ZZ) edge bond direction (green rectangle in Figure 1a). The length of the Mo−Mo edge turns out to be 0.317 nm, which corresponds to the equilibrium lattice parameter of MoS_2 with hexagonal crystal structure.[25] This result indicates that the MoS_2 lattice is not perturbed in this region. Moreover, the absence of holes[26] and folds[27] formation during the measurements, which could compromise our results, ensures that the quality of the MoS_2 flakes is

DOI: 10.1021/acs.nanolett.7b03627
Nano Lett. 2017, 17, 7021−7026

maintained when operating the microscope at 200 kV, as has been previously reported.[28,29]

Strain-Dependent Edge Structure in a MoS_2 Flake. Figure 2a displays a AC HAADF-STEM image taken in the region around the transition from three to two MLs in the [0001]-oriented MoS_2 flake. The difference in contrast separates the 3MLs (brighter) and 2MLs (darker) regions (details on the thickness measurements can be found in section SI–IV). To map the strain field around the edges of MoS_2, the GPA method has been applied.[30] The basic idea of the GPA technique is to measure local phase distortions, which can be directly linked to any distortion in the lattice fringes in the atomic-resolution HAADF image with respect to a reference. The corresponding strain fields can be then calculated by tacking the derivative of the displacement field.[31,32] In this analysis, the scan distortions introduced during the STEM data acquisition have been corrected (see sections SI and SII for further details about this procedure). The phase image (Figure 2d) was calculated for the set of (01−10) lattice fringes (Figure 2c), evaluated from the fast Fourier transform (FFT); see Figure 2b. The phase image exhibits a discontinuity from 0 to $-\frac{\pi}{5}$ around the transition from 3MLs to 2MLs. Taking the x−axis parallel to [−12−10], the corresponding strain field is shown in Figure 2e.

Crucially, from the strain field map (Figure 2e) we observe a region exhibiting tensile strain, whose value ranges between 2% and 4%, localized exactly at the transition between the regions with 2MLs and with 3MLs. More specifically, such transition region is defined by the intersections of the family of planes {1100} and {1−210}. The atomic terminations of these two families of planes are known as zigzag (ZZ) and armchair (AC) configurations, respectively, and are represented in Figure 2f. Note that when two ZZ edges merge, the resulting junction defines the minimal unit of an AC edge. We find that the ZZ edges exhibit tensile strain ranging between (2 ± 0.5) % and (4 ± 1) %, where the later value arises at the junctions between two ZZ edges (that represents a short AC edge). However, the longer AC edge (labeled as γ) appears under a tensile strain of around (2 ± 0.5) %. The corresponding strain profiles are shown in Figure SI-4 and section SI–IV. Note that here, we use a Fourier mask that leads to a spatial resolution of 0.5 nm. This choice represents an appropriate balance between smoother strain fields but worse spatial resolution (achieved with a small mask) and better spatial resolution but with a higher level of fluctuation. See section SI–III for further details about the interplay between spatial resolution and signal-to-noise ratio.

The appearance of such localized strain at the ZZ and AC edges could be related to the edge relaxation mechanism itself, induced by the adjustment of the bond length and bond angles of the edge atoms.[33] In this scenario, the MoS_2 sheets generated by mechanical exfoliation initially have an excess of energy. Therefore, the free-edges (S−Mo−S) of the MoS_2 flakes are originated with stress. Subsequently, the MoS_2 sheet relaxes to reduce this excess of energy. Theoretical calculations of the elastic properties of phosphorene nanoribbons[34] reported a similar result, where the energy relaxation modifies the atomic arrangement of AC and ZZ edges, resulting into a tensile stress along the ZZ and AC edges consistent with our findings here. Moreover, we also found that this relaxation mechanism is translated into an out-of-plane distortion[35] (see sections SI–III for further details).

EELS Characterization of Electronic Properties of MoS_2 Flakes. To obtain further insight on the effects of edge strain on the resulting electronic behavior, we have carried out a direct correlation experiment by means of an electron energy loss spectroscopy (EELS) analysis.[36] A monochromated electron source operating at 60 kV, which achieves an energy resolution of around 30 meV, was used for these measurements. A crucial advantage of EELS is that it allows achieving high-energy resolution while simultaneously leading to competitive spatial resolution.[37] Figure 3a displays a low-magnification HAADF-STEM image taken in the same region where the strain measurements were performed (see Figure 2a). Subsequently, point-by-point EELS spectra were recorded at different locations in the boundary region between 2MLs and 3MLs, indicated by the points S1 to S4 in Figure 3a. We focused on the low-loss energy region, ranging between electron energy losses of 0 and 4 eV. The most-distinctive features of the EELS spectra (Figure 3b) are the presence of two relatively narrow peaks, located at around 1.89 eV (peak A) and 2.05 eV (peak B), respectively. These two peaks in the MoS_2 EELS spectra can be interpreted as arising from the direct exciton transitions, specially due to band splitting effects induced to interlayer interaction and spin−orbit coupling.[9,38,39] Our measurements for the position of these peaks are consistent with previously experimental[40] and theoretical studies.[41] We further quantify the properties of these exciton peaks by means of a fitting procedure, in which a double Gaussian is used for the signal, combined with a quadratic polynomial for the background. The comparison between the EELS measurements and the resulting fits is shown in Figures 3c–f, where we also show the two Gaussian peaks, denoted by peak A and peak B, with the background subtracted.

One factor that is known to affect the peaks' width is the thickness of the MoS_2 layers.[40] Moreover, it is conceivable that the strain localized at the interface (see Figure 2e) might also induce variations in these widths. To investigate the interplay between these two effects, we have recorded EELS spectra at two additional locations (see Figure SI-6 in sections SI–VII), labeled by T1 (in 2 MLs region) and T2 (in 3 MLs region) in Figure 3a. Because these EELS spectra correspond to regions far from the boundaries, no effects associated with edge strain are expected to arise.

By comparing the peak A (and B) fwhm value between points T1 and T2, we find that it increases by around 70% (and 30%, respectively); see sections SI–VII. However, when comparing the fwhm values of peak A (B) between the points S1 and S3 (see Figure 4) (that is, just before and after crossing the interface where, in addition to the different thicknesses, we must also account for the possible effects of strain), we find that the increase is now around 30% (15%). Therefore, we observe a nontrivial dependence of the fwhm values of the two exciton peaks at the interface region, which cannot be accounted purely by the change in thickness and, at least partly, should be understood in terms of the interface strain. This remarkable correlation highlights the deep connection between structural and electronic properties of MoS_2, which can be tuned layer by layer. In this respect, new theoretical calculations would be required to fully disentangle the contribution of the various physical mechanisms that contribute to the exciton peak broadening, especially the interplay between the tensile strain at the edge and the layer thickness variation.

Concerning the peak positions as determined from the fit, we find values of 1.89 and 1.88 eV for peak A and 2.05 and 2.08 eV

DOI: 10.1021/acs.nanolett.7b03627
Nano Lett. 2017, 17, 7021−7026

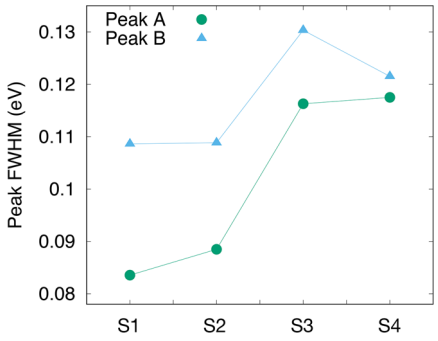

Figure 4. Variation of the fwhm of peaks A and B along this transition region, where measurements corresponding to the points labeled as S1 to S4 in Figure 3a are shown.

for peak B in the regions with two and three MLs, respectively. We therefore find that for peak B there is a clear difference in peak position between the two regions. This behavior could be understood as a direct consequence of the specific crystalline structure of MoS_2. Indeed, for an odd number of MoS_2 layers, the crystal belongs to the noncentrosymmetric D_{3h} space group. However, for an even number of layers instead, the crystal belongs to the D_{3d} space group, which is characterized by inversion symmetry.

Strain Dependence of Free-Edge Curvature. Strain-dependent edge structures also arise at the interface between the MoS_2 flake and the vacuum, the so-called free edges. Figure 5 illustrates a AC HAADF-STEM image taken in a region that

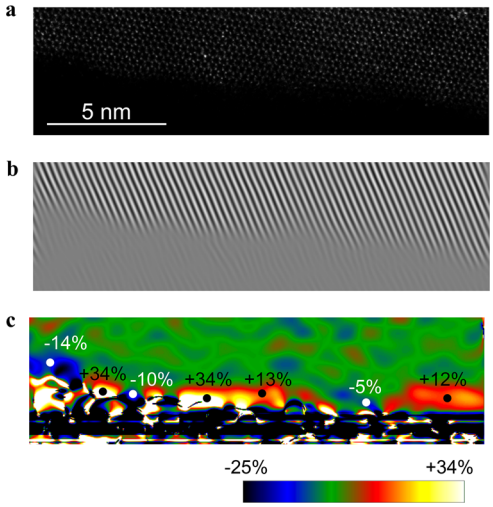

Figure 5. (a) AC HAADF−STEM image of a region exhibiting a free edge of MoS_2. (b) From the filtered lattice fringes, we can clearly identify concave and convex terminations. (c) The ε_{xx} strain component indicating the presence of compressive (tensile) strain in the concave (convex) region.

only exhibits ZZ edge terminations. Moreover, as can be seen in the filtered lattice fringes image (Figure 5b), this free edge alternates concave and convex regions. These opposite-curvature regions are originated during the mechanical exfoliation process. By following the same procedure described before, the resulting strain field map allows us to distinguish regions with alternating localized compressive and tensile strain at the ZZ edges. In particular, the concave regions exhibit a compressive strain, while for the convex ones, a tensile strain is exhibited. Moreover, as compared to the strain values reported at the interface between 2MLs and 3MLs (see Figure 2e), here the levels of strain reached are higher, with values up to around +30% in the convex regions and down to around −14% in the concave regions. These results suggest that the possibility of exploiting the free edge curvature to turn tensile into compressive strain could provide a novel handle to tune the electronic properties of layered materials.

To summarize, controlling and understanding the formation of localized strain at the edge structures of TMD materials is of great importance toward the customization of their electronic properties. Here, by combining aberration-corrected TEM with the geometrical phase analysis method, we have quantified the edge structures and elastic properties of MoS_2 flakes. We find that the relaxation of the ZZ and AC edge structures leads to the appearance of a tensile strain, with magnitude ranging between 2% and 4%. This implies that the tensile strain can lead to the elastic distortion of the edge. Moreover, the EELS analysis performed at the same transition region highlights an increase of the exciton A and B peak widths by around 30% and 15%, respectively, that can at least partly be explained by the presence of such tensile strain at the edges. However, this broadening of the exciton peaks also receives contributions from the change of thickness of the MoS_2 layers. In this respect, new theoretical calculations would be required to fully disentangle the contribution of the various physical mechanisms that contribute to the exciton peak broadening, especially the interplay between the tensile strain at the edge and the layer thickness variation. Finally, strain measurements performed at free edges between MoS_2 and a vacuum, which exhibit convex and concave regions, demonstrate the direct interplay between interface curvature and the presence of either tensile or compressive strain. Even if here we have restricted ourselves to the analysis of MoS_2 flakes, our approach is fully general, and we plan to extend it to a comprehensive analysis of the strain-dependent edge structures in other layered materials. Our results could therefore pave the way toward the customization of electronic properties of TMD materials by means of strain-dependent edge structure.

■ ASSOCIATED CONTENT

Supporting Information

The Supporting Information is available free of charge on the ACS Publications website at DOI: 10.1021/acs.nanolett.7b03627.

Additional details on experimental methods, strain treatment and EELS spectra. (PDF)

■ AUTHOR INFORMATION

Corresponding Author

*E-mail: s.conesaboj@tudelft.nl.

ORCID

Sonia Conesa-Boj: 0000-0003-1716-184X

Author Contributions

M.T prepared the sample for TEM studies. M.M, E.O., and S.C.-B. analyzed the MoS_2 with TEM. M.T. and S.C.-B. performed the strain measurements and interpretation. M.T. performed the EELS data analysis. All of the authors contributed to the discussion of the results and wrote and commented on the manuscript. S.C.-B conceived the idea and supervised the project.

DOI: 10.1021/acs.nanolett.7b03627
Nano Lett. 2017, 17, 7021−7026

Notes

The authors declare no competing financial interest.

■ ACKNOWLEDGMENTS

M.T., L.M., and S.C.-B. acknowledges financial support from The Netherlands Organization for Scientific Research (NWO) through the Nanofront program. We are grateful to the TEM facilities of JFFC (Nagoya, Japan) where the TEM measurements were carried out. We also acknowledge Nikos Papadopoulos for providing us with the MoS_2 specimen.

■ REFERENCES

(1) Lukowski, M. A.; Daniel, A. S.; Meng, F.; Forticaux, A.; Li, L.; Jin, S. *J. Am. Chem. Soc.* **2013**, *135*, 10274.
(2) Voiry, D.; Yamaguchi, H.; Li, J.; Silva, R.; Alves, D. C. B.; Fujita, T.; Chen, M.; Asefa, T.; Shenoy, V. B.; Eda, G.; Chhowalla, M. *Nat. Mater.* **2013**, *12*, 850.
(3) Lauritsen, J. V.; Kibsgaard, J.; Helveg, S.; Topsoe, H.; Clausen, B. S.; Laegsgaard, E.; Besenbacher, F. *Nat. Nanotechnol.* **2007**, *2*, 53.
(4) Radisavljevic, B.; Radenovic, A.; Brivio, J.; Giacometti, V.; Kis, A. *Nat. Nanotechnol.* **2011**, *6*, 147.
(5) Li, M.-Y.; Shi, Y.; Cheng, C.-C.; Lu, L.-S.; Lin, Y.-C.; Tang, H.-L.; Tsai, M.-L.; Chu, C.-W.; Wei, K.-H.; He, J.-H.; Chang, W.-H.; Suenaga, K.; Li, L.-J. *Science* **2015**, *349*, 524.
(6) Yin, Z.; Li, H.; Li, H.; Jiang, L.; Shi, Y.; Sun, Y.; Lu, G.; Zhang, Q.; Chen, X.; Zhang, H. *ACS Nano* **2012**, *6*, 74.
(7) Rigosi, A. F.; Hill, H. M.; Li, Y.; Chernikov, A.; Heinz, T. F. *Nano Lett.* **2015**, *15*, 5033.
(8) Chen, Y.; Xi, J.; Dumcenco, D. O.; Liu, Z.; Suenaga, K.; Wang, D.; Shuai, Z.; Huang, Y.-S.; Xie, L. *ACS Nano* **2013**, *7*, 4610.
(9) Mak, K. F.; Lee, C.; Hone, J.; Shan, J.; Heinz, T. F. *Phys. Rev. Lett.* **2010**, *105*, 136805.
(10) Reddy, C. D.; Ramasubramaniam, A.; Shenoy, V. B.; Zhang, Y.-W. *Appl. Phys. Lett.* **2009**, *94*, 101904.
(11) Gan, C. K.; Srolovitz, D. J. *Phys. Rev. B: Condens. Matter Mater. Phys.* **2010**, *81*, 124445.
(12) Shenoy, V. B.; Reddy, C. D.; Ramasubramaniam, A.; Zhang, Y. W. *Phys. Rev. Lett.* **2008**, *101*, 245501.
(13) Jun, S. *Phys. Rev. B: Condens. Matter Mater. Phys.* **2008**, *78*, 073405.
(14) Peng, X.; Wei, Q.; Copple, A. *Phys. Rev. B: Condens. Matter Mater. Phys.* **2014**, *90*, 085402.
(15) Conley, H. J.; Wang, B.; Ziegler, J. I.; Haglund, R. F.; Pantelides, S. T.; Bolotin, K. I. *Nano Lett.* **2013**, *13*, 3626.
(16) Kibsgaard, J.; Chen, Z.; Reinecke, B. N.; Jaramillo, T. F. *Nat. Mater.* **2012**, *11*, 963.
(17) Peres, N. M. R.; Rodrigues, J. N. B.; Stauber, T.; Lopes dos Santos, J.M. B. *J. Phys.: Condens. Matter* **2009**, *21*, 344202.
(18) Peres, N. M. R. *Rev. Mod. Phys.* **2010**, *82*, 2673.
(19) Neto, A. C.; Guinea, F.; Peres, N. M. *Phys. World* **2006**, *19*, 33.
(20) Helveg, S.; Lauritsen, J. V.; Lægsgaard, E.; Stensgaard, I.; Nørskov, J. K.; Clausen, B. S.; Topsøe, H.; Besenbacher, F. *Phys. Rev. Lett.* **2000**, *84*, 951.
(21) van der Zande, A. M.; Huang, P. Y.; Chenet, D. A.; Berkelbach, T. C.; You, Y.; Lee, G. H.; Heinz, T. F.; Reichman, D. R.; Muller, D. A.; Hone, J. C. *Nat. Mater.* **2013**, *12*, 554.
(22) Gutiérrez, H. R.; Perea-Lopez, N.; Elias, A. L.; Berkdemir, A.; Wang, B.; Lv, R.; Lopez-Urias, F.; Crespi, V. H.; Terrones, H.; Terrones, M. *Nano Lett.* **2013**, *13*, 3447.
(23) Wu, Q.; Li, X.; Volinsky, A. A.; Su, Y. *Phys. Lett. A* **2017**, *381*, 1568.
(24) LeBeau, J. M.; Stemmer, S. *Ultramicroscopy* **2008**, *108*, 1653.
(25) Kang, J.; Tongay, S.; Zhou, J.; Li, J.; Wu, J. *Appl. Phys. Lett.* **2013**, *102*, 012111.
(26) Sammalkorpi, M.; Krasheninnikov, A.; Kuronen, A.; Nordlund, K.; Kaski, K. *Phys. Rev. B: Condens. Matter Mater. Phys.* **2004**, *70*, 245416.
(27) Castellanos-Gomez, A.; van der Zant, H. S. J.; Steele, G. A. *Nano Res.* **2014**, *7*, 572.
(28) Brivio, J.; Alexander, D. T. L.; Kis, A. *Nano Lett.* **2011**, *11*, 5148.
(29) Shi, Y.; Huang, J.-K.; Jin, L.; Hsu, Y.-T.; Yu, S. F.; Li, L.-J.; Yang, H. Y. *Sci. Rep.* **2013**, *3*, 1839.
(30) Hytch, M. J.; Snoeck, E.; Kilaas, R. *Ultramicroscopy* **1998**, *74*, 131.
(31) Conesa-Boj, S.; Boioli, F.; Russo-Averchi, E.; Dunand, S.; Heiss, M.; Ruffer, D.; Wyrsch, N.; Ballif, C.; Miglio, L.; i Morral, A. F. *Nano Lett.* **2014**, *14*, 1859.
(32) Warner, J. H.; Young, N. P.; Kirkland, A. I.; Briggs, G. A. D. *Nat. Mater.* **2011**, *10*, 958.
(33) Huang, Y.; Ling, C.; Liu, H.; Wang, S. *RSC Adv.* **2014**, *4*, 6933.
(34) Sorkin, V.; Zhang, Y. W. *Nanotechnology* **2015**, *26*, 235707.
(35) Ivanovskaya, V. V.; Wagner, P.; Zobelli, A.; Suarez-Martinez, I.; Yaya, A.; Ewels, C. P. *Carbon Nanostructures* **2012**, 75.
(36) Arenal, R.; Stephan, O.; Kociak, M.; Taverna, D.; Loiseau, A.; Colliex, C. *Phys. Rev. Lett.* **2005**, *95*, 127601.
(37) Garcia de Abajo, F. J. *Rev. Mod. Phys.* **2010**, *82*, 209.
(38) Splendiani, A.; Sun, L.; Zhang, Y.; Li, T.; Kim, J.; Chim, C.-Y.; Galli, G.; Wang, F. *Nano Lett.* **2010**, *10*, 1271.
(39) Fan, X.; Singh, D. J.; Zheng, W. *J. Phys. Chem. Lett.* **2016**, *7*, 2175.
(40) Nerl, H. C.; Winther, K. T.; Hage, F. S.; Thygesen, K. S.; Houben, L.; Backes, C.; Coleman, J. N.; Ramasse, Q. M.; Nicolosi, V. Probing the local nature of excitons and plasmons in few-layer MoS_2. *npj 2D Materials and Applications* **2016**, *2*, 1 DOI: 10.1038/s41699-017-0003-9.
(41) Komsa, H. P.; Krasheninnikov, A. V. *Phys. Rev. B: Condens. Matter Mater. Phys.* **2012**, *86*, 241201.

DOI: 10.1021/acs.nanolett.7b03627
Nano Lett. 2017, 17, 7021−7026